JOURNAL OF MATERIALS SCIENCE **38** (2003) 3579–3589

# Effects of gravitational orientation on the microstructural evolution of gas tungsten arc welds in an Al-4 wt% Cu alloy

N. KANG*, J. SINGH*, A. K. KULKARNI‡
*Department of *Materials Science and Engineering and ‡Mechanical and Nuclear Engineering, The Pennsylvania State University, University Park, PA 16802, USA*
*E-mail: singh@matse.psu.edu*

Gas tungsten arc (GTA) welds on Al-4 wt% Cu alloys were investigated to determine effects of gravitational orientation on the weld solidification behavior. A bead-on-plate welding was performed by varying the relation between the arc translation direction and gravity vector, e.g., parallel-up, parallel-down, and perpendicular orientations. A solidification rate ($V_S$) was calculated from the measured grain orientation, and a thermal gradient ($G_L$) was estimated from the observed weld pool shape following a linear relation. A primary dendrite spacing ($\lambda_1$) decreased continuously from the s-l boundary to the weld pool surface regardless of the gravitational orientations. Larger $\lambda_1$ for the parallel-up weld was observed near the boundary and surface than that of the perpendicular and parallel-down welds, which is believed to be associated with a smaller $G_L$ due to larger weld pool dimension and with different solidification morphology. A solidification morphology and orientation in the perpendicular and parallel-up welds was comparable with a loss of columnar directionality near the weld surface and a continuous grain orientation. However, the parallel-down weld exhibited more columnar structure near the surface, which might be associated with the larger $G_L$ and relatively mild convection flows. Outward convection flows in the parallel-down weld might be inhibited because of its reverse direction with respect to the gravity vector. This resulted in abnormal 'S' shape of the trailing s-l interface and the $V_S$, which was receded toward the weld pool center. Based on these findings, significant influence of gravitational orientation resulted in the variation on the weld pool shape associated with convection flows, which in turn affected solidification orientation/morphology and the primary dendrite spacing. 

## 1. Introduction

A welding process in microgravity and a circumferential pipe welding in the terrestrial environment are expected to play a role in the space construction and in the huge structural welding, respectively. For the performance of these processes, it is necessary to understand effects of gravitational level and orientation on the welding phenomena, such as the convection flow and weld pool dimension, the microstructural evolution, and the segregation. There are a number of resources reporting the gravitational effects on the weld pool geometry and convection flows [1–4]. During unidirectional solidification, the absence of gravity-driven convection flows increased the primary dendrite spacing ($\lambda_1$) in Pb-Sn alloys [5] and Al-Cu alloys [6], but it also showed an opposite result as a decrease of the $\lambda_1$ in Pd40Ni40P20 alloys [7]. No gravitational effects on the macrosegregation were reported in the Al-Cu alloy [8], however Liu *et al.* reported lower P solute contents in the primary phase as gravitational level decreased [7]. For an Nd-YAG laser welding on a 304 stainless steel, a high-gravity produced an equiaxed dendritic microstructure transformed from a radial columnar structure in the low-gravity welds [9]. Fine equiaxed grains located along the s-l boundary disappeared in the high-gravity due to enhanced convection in GTA welded Al alloys [10]. However, systematic studies of the gravitational effect, either orientation or level, on the weld microstructural evolution have not been conducted to the best of the authors' knowledge for solving the above controversy.

The unidirectional solidification has been studied more theoretically and systematically than the weld solidification because it is absent of the interacting surface tension-driven and electromagnetic forces existing in the weld pool. In unidirectional solidification experiments, solidification parameters such as thermal gradient ($G_L$) and solidification rate ($V_S$) could be controlled independently. Therefore, the microstructural dependence on either $G_L$ at constant $V_S$ or $V_S$ at constant $G_L$ was studied. During the weld solidification, columnar-dendritic structures are the frequently observed

morphology. The microstructural size of dendrites characterizes the solute segregation pattern that largely determines the properties of the material [11, 12]. One of the most important quantities used to describe dendritic structures in columnar growth is the primary dendrite spacing ($\lambda_1$). Significant amount of unidirectional solidification studies have been conducted to characterize the $\lambda_1$ as a function of solidification conditions [13–17]. Most experimental studies have shown that the $\lambda_1$ decreases as the solidification parameter increases. Equation 1 indicates a $\lambda_1$ behavior as a function of the solidification parameters, where $C_1$ is a kinetic constant that is characteristic of the alloy system under consideration. The constants $a$ and $b$ were defined respectively as 0.5 and 0.25 from the theoretical models [18–20].

$$\lambda_1 = C_1 G_{\mathrm{L}}^{-a} V_{\mathrm{S}}^{-\mathrm{b}} \tag{1}$$

The solidification behavior of the weld has also been studied by applying rapid solidification theories [21]. Kurz, Giovanola, and Trivedi (KGT) developed a theoretical model for dendritic growth under rapid solidification conditions [22]. It shows that the solidification rate ($V_{\mathrm{S}}$) is the key factor in microstructural size. According to the KGT model, the experimentally measured $\lambda_1$, as a function of solidification rate, tends to obey the relationship,

$$\lambda_1^2 V_{\mathrm{S}} = \text{constant}. \tag{2}$$

Equation 2 is the relation observed in Al-Fe binary alloys under the solidification rate between 0.1 and 6.0 m $s^{-1}$ [23]. The solidification rate ($V_{\mathrm{S}}$) was obtained by measuring the grain orientation in a longitudinal cross-section through the center-plane of the welded track, as shown in Fig. 1. The orientation of the microstructure tends to be perpendicular to the local solid-liquid interface because the grains are known to grow parallel to the direction of heat dissipation. Therefore, the orientation of the grain boundary or that of the interdendritic phase was measured with respect to the arc translation direction. The relationship between the arc translation rate ($V_a$) and the local solidification rate ($V_{\mathrm{S}}$) is indicated as:

$$V_{\mathrm{S}} = V_a \cos\theta \tag{3}$$

where $\theta$ is the angle between the vectors representing $V_{\mathrm{S}}$ (parallel to the microstructure) and $V_a$ (parallel to the arc translation). The details of this method have been described elsewhere [21, 23, 24]. Between the fusion boundary and the weld pool surface, the solidification rate varies from zero to a maximum depending on the size and shape of the melt pool. The above observations have been applied successfully to the welding microstructures of the Al-Cu alloys [25]. However, Equation 3 has not been exploited to investigate the influence of gravitational orientation on the weld solidification and microstructural behavior.

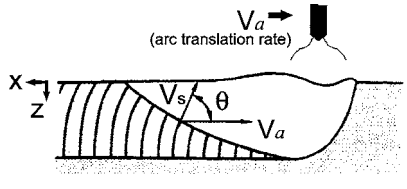


*Figure 1* Schematic diagram of the molten pool at the center-plane of the welded track.

Despite of these studies, understanding the factors that control the $\lambda_1$ in the weld is limited. This is mainly because the $G_{\mathrm{L}}$ cannot be precisely controlled during the welding process and the weld pool contains interacting convection flows. Even in the well-controlled unidirectional solidification, there was a wide allowable range of primary spacing for a given growth condition [13, 17, 26]. In the longitudinal cross-section (Fig. 1), the weld structure can contain many of the measured $\lambda_1$ corresponding to the spacing away from the closest packing direction of dendrites. A liquid weld pool contains convection flows that have not been considered in Equations 1 and 2. The convection flow plays a significant role in influencing the microstructure as well as the weld pool shape. In the presence of significant convection flows, the liquid weld pool may loose its steady state formation (fluctuations) and its regular advance with time. However, the fluctuations seemed to perturb the dendrite growth only locally and the mean spacing in these perturbed regions did not vary to a significant degree [21]. For these reasons, the theoretical and experimental relations on the $\lambda_1$ will be carefully used during the quantitative analysis.

The objective of the present study is to investigate effects of gravitational orientation on the GTA weld microstructural evolution in Al-4 wt% Cu alloys. This study will be focused on the behavior of solidification morphology, orientation, and primary dendrite spacing ($\lambda_1$) as a result of the weld pool shape variation with respect to the gravitational orientation. Growing evidence suggests that gravity plays an influential role in weld pool surface deformation, which in turn affects weld pool shape [27]. Considering the effect of convection flows on the $V_{\mathrm{S}}$ and $G_{\mathrm{L}}$, the solidification parameters with respect to the welding orientation will be examined in this study. Solidification orientation and $\lambda_1$ will be measured at the longitudinal cross-section of the center-plane of the welded track. These measurements will be used to calculate the $V_{\mathrm{S}}$. The $G_{\mathrm{L}}$ will be estimated from the observed weld pool shape. The investigation on the $V_{\mathrm{S}}$ and $G_{\mathrm{L}}$ will extend the understanding of the solidification morphology and microstructural size ($\lambda_1$) as a function of the gravitational orientation. Al-Cu system was chosen for this study because of its most available experimental results and well-defined physical properties. For the future study, this alloy system also helps amplify the gravitational effects on solute segregation due to its high-density difference of solute atoms.

## 2. Experimental details

To examine effects of gravitational orientation on the microstructural evolution, the experiments were designed such that the relation between the gravity vector and the arc translation direction was varied. Fig. 2 depicts the welding orientations that were used to simulate different gravitational conditions, e.g., welding upward in a direction opposing gravity (parallel-up or

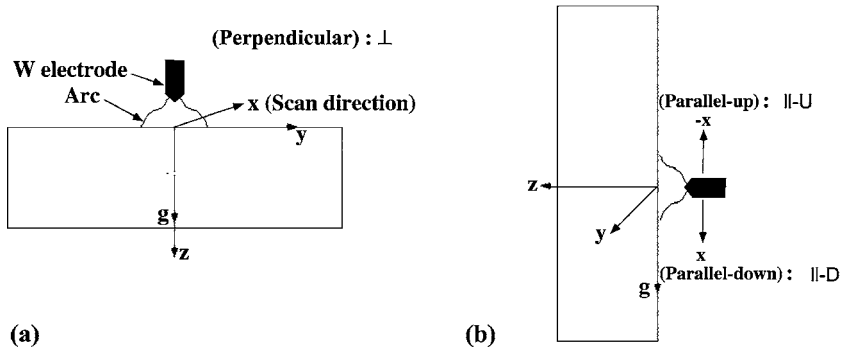


*Figure 2* Welding direction: (a) perpendicular (⊥) orientation to gravity and (b) parallel-up (ll-U) and parallel-down (ll-D) orientations to gravity.

ll-U weld), welding downward in the direction of gravity (parallel-down or ll-D weld), and welding perpendicular to the direction of gravity (perpendicular or ⊥ weld).

The welding conditions were selected from the reasoning gained in the previous Ni study [27]: Gravitational effects on the weld pool shape were more significant at slow translational velocity ($V_a$) and high arc power. Based on the results, the present study will be focused on the specific welding conditions (slow $V_a$ and high power) for the purpose of magnifying the gravitational effects on the weld pool shape and microstructure. Bead-on-plate welds were produced on the Al-4 wt% Cu alloy autogenously for a constant direct current 185A and a variable arc voltage of 16.5 V (±0.2 V). The tungsten-2% thorium electrode was held stationary and the sample plate mounted on the working table being made of the aluminum 2024 alloy was translated with a constant velocity 3 mm $s^{-1}$. The Al-Cu alloy was prepared by vacuum induction melting and casting. The cooling was accelerated by introducing argon into the furnace. In order to eliminate inhomogeneities at the surface and possible contamination from the mold, the ingot dimensions were reduced by machining off the surface. After polishing the surface on 1000 grit SiC paper, the sample plate had dimensions of 50 mm × 150 mm × 6.5 mm. The welds were sectioned and mounted along the direction of the weld (top view), along the weld center-plane (longitudinal cross-section), across the weld (transverse cross-section). The macro- and microstructure of the weld was studied by using conventional optical microscopy and scanning electron microscopy (SEM).

Microstructural investigation was focused on the characterization of primary dendrite arm spacing ($\lambda_1$). The $\lambda_1$ was measured from the microstructure of a cross-section taken parallel to the growth direction. The $\lambda_1$ was defined from the number of dendrite centers in the longitudinal cross-section, which intersect a line of fixed length drawn along the direction of closest primary dendrite packing. The average of ten to fifteen line measurements was taken after remitting the maximum and minimum values obtained.

## 3. Results and discussion

The present study is evolved from the previous Ni GTA welding study [27] with the following hypothesis: As gravitational orientation varies, the weld pool shape is changed as a result of the variation on convection flows. It is believed that the convection flow is associated with solidification rate ($V_S$) and thermal gradient ($G_L$). Therefore, the weld microstructure and solidification orientation will be influenced as a function of the gravitational orientation. In this study, the ll-U weld is expected to have larger weld pool area due to more significant convection flows than the ll-D weld. Larger weld pool in the ll-U weld will produce the smaller $G_L$ and cooling rate, which will be associated with the loss of columnar structure and larger $\lambda_1$.

### 3.1. Weld pool geometry

An analysis of the gravitational effects demonstrated that the weld pool geometry was varied considerably by changing welding orientation depicted in Fig. 2. Table I shows the average size of the depth, the width, the depth to width ratio, and the transverse cross-sectional area of the fusion zone (FZ). The ll-U weld had 15 percent deeper penetration and 22 percent larger FZ area than those of the ⊥ and ll-D welds. The width and the depth to width ratio of the welds, in contrast, showed little to no variation on the welding orientation. These results were comparable with the previous investigation of the GTA welds on nickel [27]. During $CO_2$ laser welding on the polypropylene, it was reported that the ll-U weld showed approximately 15% increased penetration [28]. Foley *et al.* also reported that the $CO_2$ laser welding on the low carbon steel produced approximately 20% deeper penetration in the ll-U weld than that in the ll-D weld [2]. More penetration of the ll-U weld in the present study was associated with more depressed weld pool surface than the ⊥ and ll-D welds. Additional details are discussed in reference [27].

The FZ and HAZ (heat affected zone) on the top-view are indicated for various welding orientations in Fig. 3. Although it is very difficult to define the HAZ

TABLE I Measured weld pool shape (FZ) as a function of gravitational orientation

| | Depth (mm) | Width (mm) | Depth/width | Area ($mm^2$) |
|---|---|---|---|---|
| ⊥ | 2.35 ± 0.1 | 6.60 ± 0.1 | 0.36 ± 0.03 | 11.0 ± 0.4 |
| ll-U | 2.75 ± 0.1 | 6.75 ± 0.2 | 0.41 ± 0.05 | 13.6 ± 0.5 |
| ll-D | 2.35 ± 0.1 | 6.50 ± 0.1 | 0.36 ± 0.03 | 10.6 ± 0.3 |

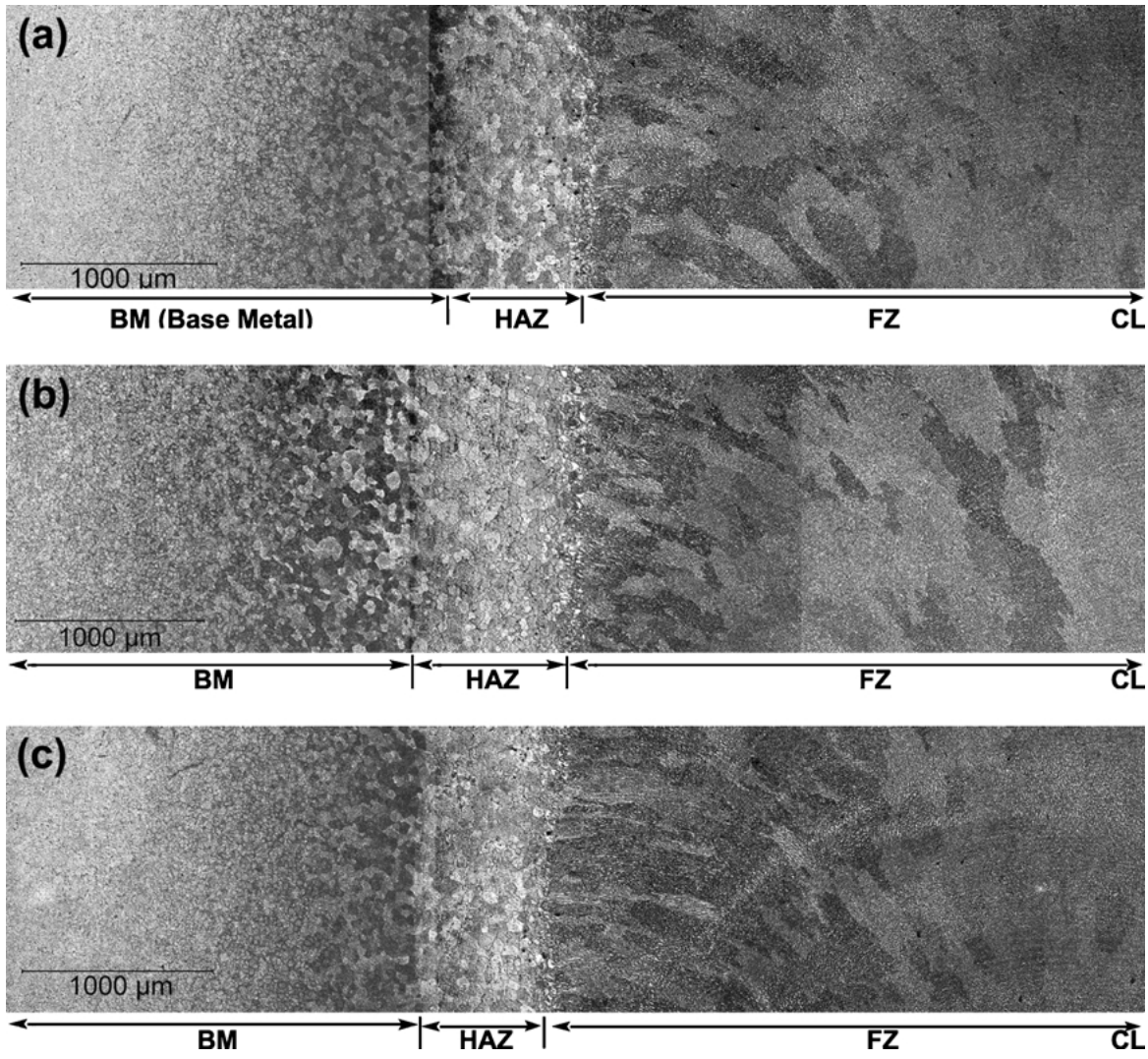


*Figure 3* Weld bead structure in the (a) perpendicular, (b) parallel-up, and (c) parallel-down welds. 'CL' stands for the centerline of the weld pool on the top view.

area quantitatively, the ∥-U weld showed larger HAZ area than that for the ⊥ and ∥-D. Fig. 3 showed a wider HAZ width for the ∥-U than that for the ∥-D and ⊥. This result indicates that the ∥-U weld not only promoted the convection flows significantly enough to impact the FZ shape but also transferred the heat more effectively to the FZ boundary. That is why the ∥-U weld produced a larger HAZ area although heat input, which is defined as the ratio of arc power and arc translation rate, remained constant during the study.

There are several observations found in the literature that can explain the behavior of the weld pool shape with respect to gravity: (i) weld pool surface depression was more significant for the ∥-U weld, therefore developing the deeper penetration [27], (ii) the weld pool area exceeded the surface tension limit to hold the mass of liquid metal, therefore changing the weld pool shape with respect to gravitational orientation [2, 3, 29], (iii) surface tension-driven convection force and/or gravitational buoyancy force were directly impacted as the gravitational level varied [4, 30]. Regardless of the effects due to the convection or surface deformation, it is fairly certain that the $G_L$ and cooling rate (CR) in the weld pool will be varied with respect to the gravitational orientation. It is because the weld pool shape varied under the constant heat input. Furthermore, it is anticipated that the variation of the $G_L$ and CR will have an influence on the solidification morphology and primary dendrite spacing that will be presented on the next Sections 3.2. and 3.3.

## 3.2. Weld solidification morphology and orientation

### *3.2.1. Weld solidification morphology*

Considering significant gravitational effects on the FZ geometry, the solidification morphology was investigated to study the gravitational influence on the weld macro- and microstructure. As shown in Fig. 3, the columnar grains grew from the solid-liquid boundary, and 'axial' or 'stray-like' grain structures were observed along the central region of the weld surface with no indication of equiaxed grains. The axial and stray grain structures have been reported in the GTA welded Al alloys [31]. A band type of weld bead was also observed irrespective of the gravitational orientation. It suggests that significant convection flows exist in the liquid weld pool [21]. From the top view, variation in the macroscopic grain structure was not evident with respect to the gravitational orientation.

Microstructural studies on the solidification morphology were conducted from the grain structures taken at the higher magnification, which are shown in Fig. 4. The SEM photographs were taken from the longitudinal cross-section at the center-plane. A columnar-dendritic growth pattern (dark colored) can be seen with a light structure present in the interdendritic regions. At the aluminum rich corner of the binary Al-Cu system, the dendritic matrix corresponds to the Al-rich phase and the interdendritic region to the eutectic mixture. The columnar grains from the fusion boundary had a coarse and elongated shape for all welding orientation (Fig. 4a–c). As the solidification proceeded, the grain became finer continuously toward the weld surface as indicated in Fig. 4d–f. The ∥-D grains on the surface remained the elongated shape. However, the ∥-U grains mostly lost a directionality of the columnar structure, i.e., approaching the equiaxed structure, although it still seems to have the columnar structure because it maintains the directionality. The grain shape of the ⊥ weld is between that of the ∥-U and ∥-D grains. More detailed explanation on the morphological observation including the solidification orientation is discussed in the next Section 3.2.2.

### 3.2.2. Weld solidification orientation

Further investigation was conducted on the longitudinal cross-section to determine the gravitational effects on the weld solidification orientation. The solidification orientation was measured by the angle $\theta$ between the columnar growth direction and the arc translation direction as illustrated in Fig. 1. For the ⊥ and ∥-U welds, the orientation of the columnar-dendritic grains decreased continuously from the fusion boundary to the weld pool surface. However, the ∥-D weld showed an abnormal behavior of the orientation between the boundary and the surface. Fig. 5a depicts the grain orientation measured through the thickness at the center-plane of the welded track. The orientations of the columnar grains with respect to the arc translation direction were converted to the solidification rate ($V_S$) using Equation 3. Fig. 5b shows the calculated $V_S$, which is correlated with the grain orientation. The ∥-D weld clearly exhibited an abnormal 'S' shape of the $V_S$ while the ⊥ and ∥-U welds had continuously increasing $V_S$ from the boundary to the surface. This result has not been reported in the literature to the best of the authors' knowledge. Except for the abnormal $V_S$ curvature of the ∥-D weld, all welding orientations showed almost same

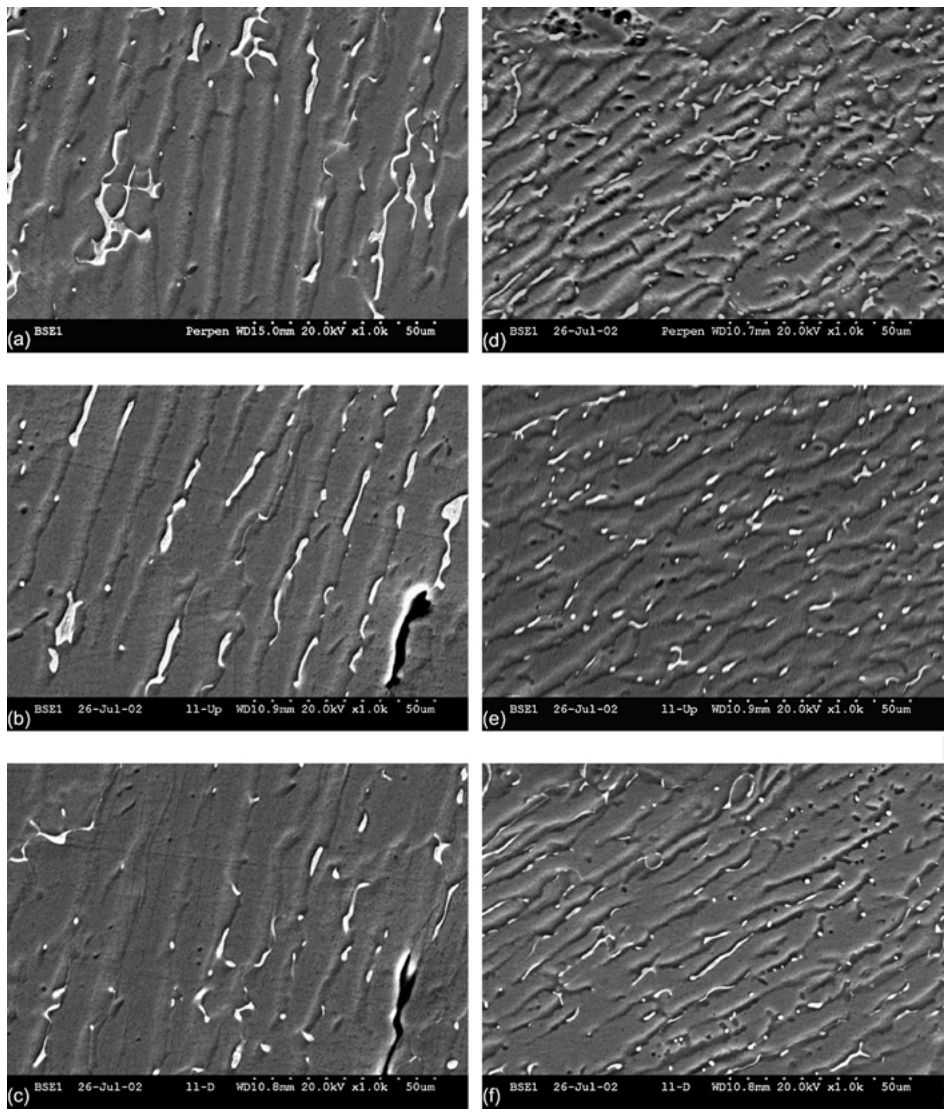


*Figure 4* Representative microstructures of the Al-4 wt% Cu welds for various welding orientation at two locations; near the fusion boundary for the (a) ⊥, (b) ∥-U, (c) ∥-D weld, and near the weld pool surface for the (d) ⊥, (e) ∥-U, and (f) ∥-D weld.

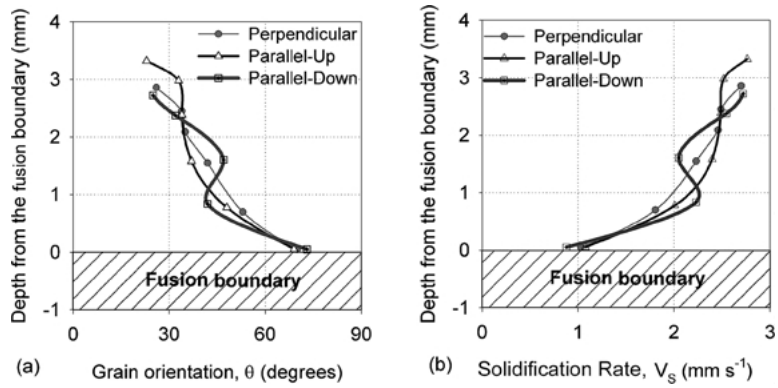


*Figure 5* Effects of gravitational orientation on the solidification behavior: (a) the measured angle $\theta$ between $V_S$ and $V_a$ and (b) the calculated $V_S$ with respect to the depth from the fusion boundary.

values of the $V_S$ at both the ends of the fusion boundary and the weld pool surface. The maximum $V_S$ on the surface was controlled by the arc translation rate and the minimum $V_S$ was limited by the fusion boundary. In Fig. 5a and b, the maximum depth from the fusion boundary indicates the larger values compared with the weld pool depth shown in Table I. It occurred because the weld pool surface was not flat, i.e., piling-up in the center of the weld pool and undercutting near the s-l boundary. As a reference, the weld pool depth in Table I was measured from the weld pool bottom to the unmelted surface away from the FZ.

The variation of the solidification morphology and orientation will be explained by using a concept of convection flows and solidification parameters ($G_L$ and $V_S$) with respect to the gravitational orientation. It is worth mentioning that the solidification parameters are associated with the convection flow. Therefore, it is necessary to understand the convection in advance within the liquid weld pool of Al alloys. Convection flows in the liquid weld pool head outward in Al alloys because the outward flow by the combined forces (surface tension-driven force and buoyancy force) dominates over the inward flow by the electromagnetic force [32].

For further understanding, the convection flow within the weld pool is illustrated for both the ll-U and ll-D welds in Fig. 6. It includes the shape of the trailing s-l interface and the dimension of the weld pool, which is associated with the convection flow. The shape and dimension of the weld pool has been exaggerated by scaling for the purpose of comparison between the ll-D and the ll-U weld. The thermal gradients ($G_L$) in x- and z-directions are also indicated as separate graphs for explaining the solidification morphology later in this section and the primary dendrite spacing ($\lambda_1$) in the next section. During the ll-U weld, gravity may promote a flow of liquid metal toward the rear of the weld pool. Due to its promotion on the outward convection flow, the trailing s-l boundary will exhibit a circular shape with no abnormal trend (Fig. 6a). So does the $V_S$ because it is directly related to the shape of the trailing s-l interface. In contrast, the outward convection flow in the ll-D weld may be inhibited because its direction from the center to the rear of the weld is opposite to the gravity vector. The inhibited outward convection flows will produce the receded s-l interface toward to the center of the weld pool as shown in Fig. 6b. The receded interface will also influence on the abnormal 'S'

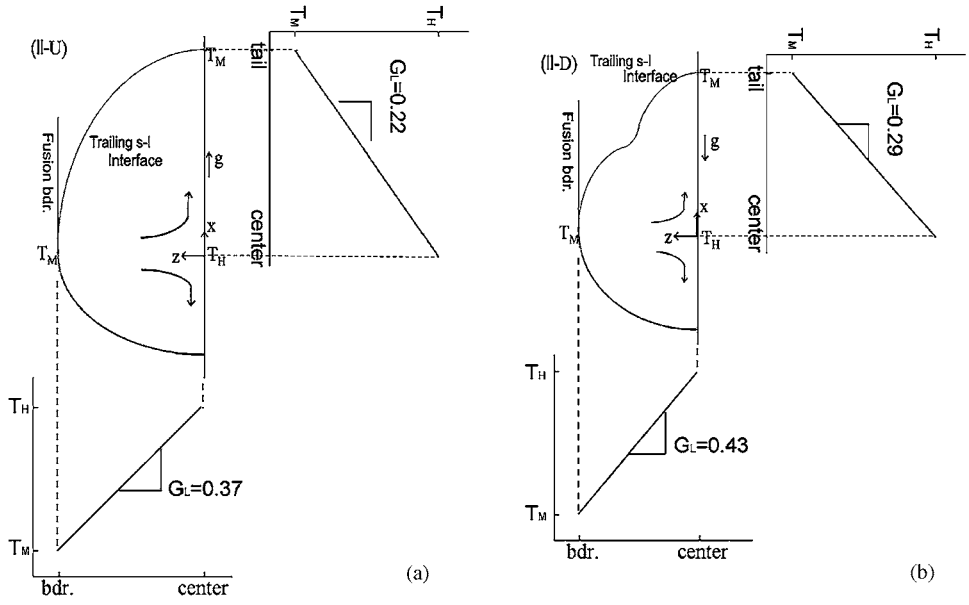


*Figure 6* Illustration of the trailing s-l interface for the ll-U (a) and the ll-D weld (b). The schematic diagrams to estimate the $G_L$ (K $\mu m^{-1}$) are located on the right-hand side and on the bottom of the weld pool illustration.

shape of the solidification orientation and $V_S$ as shown in Fig. 5a and b, respectively. Behavior of the ⊥ weld lies between the ǁ-U and ǁ-D cases.

The degree of convection flows in the liquid weld pool has also been known to change the dendrite spacing and orientation [33]. Stronger convection caused the dendrite fragmentation and changed the dendrite morphology from the elongated structure to the equiaxed one [34]. This result indicates that the ǁ-U weld may have more significant convection flows than the ǁ-D and ⊥, thereby influencing the morphology, i.e., losing the directionality of the columnar structure near the weld pool surface, as shown in Fig. 4d–f. Furthermore, this variation of the convection flow will affect the solidification parameters because the convection flow influenced the solidification morphology and orientation in the present study.

More systematic studies on the solidification morphology have been conducted for the thermal gradient ($G_L$) and solidification rate ($V_S$) at the s-l interface [35] than for the convection flow. The $G_L$ and $V_S$ depends on the heat input (arc power/arc translation rate) and weld pool shape, more specifically on the shape of the trailing s-l isotherm (interface) and on the distance between solidus and liquidus isotherms. Clarke *et al.* [36] predicted the columnar-to-equiaxed grain transition (CET) by using a numerical simulation to achieve the $G_L$ and $V_S$ on Al-Cu alloys. The welding conditions producing a low $G_L$ and sufficiently high $V_S$ were favored for a CET. In the present study, the $V_S$ varied considerably depending on the position at the s-l interface as shown in Fig. 5b. The $V_S$ was at its minimum at the fusion boundary and it increased closer to the weld pool surface. Therefore, there is a transition of the morphology from the columnar-dendritic structure near the boundary (Fig. 4a–c) to the loss of directionality of the columnar structure near the surface (Fig. 4d–f). In order to explain more loss of columnar directionality near the ǁ-U weld surface, it is speculated that the ǁ-U weld must have a lower $G_L$ than the ⊥ and ǁ-D welds. The lower $G_L$ in the ǁ-U weld was associated with its larger FZ area mentioned in the previous section, and this is further illustrated below. This result was comparable with the analysis of Clarke [36].

The comparison of the $G_L$ between the ǁ-U and ǁ-D welds can be visualized more clearly from the illustration on thermal behavior (Fig. 6). $T_H$ is the highest temperature in the center of the weld pool surface and $T_M$ is the melting temperature. Both temperatures are assumed to be constant regardless of the welding orientation because the heat input remained constant during the study. It is also assumed that there is no vaporization occurring during the welding. Under these assumptions, the highest temperature ($T_H$) was set to 1900 K lying between the melting temperature ($T_M \approx 870$ K) and vaporization temperature ($T_V \approx 2700$ K) of Al alloys. In the literature [32, 37], the highest temperature on 6061 Al alloys was found to be approximately 1900 K during the GTA welding with a similar welding power. At the end of welding track, the length between the center and the tail of the weld bead was measured for use in the $G_L$ calculation in the x-direction. Measured depth of the FZ (Table I) was used for the $G_L$ calculation in the z-direction. The linear temperature distribution between $T_H$ and $T_M$ was applied to simplify the calculation. The slope of the linear lines represents $G_L$ in Fig. 6. This simplification may be contrary to the normal understanding that the $G_L$ increases as the weld pool center is approached because of the intense heat in the center and the heat dissipation away from the fusion boundary. Therefore, the $G_L$ in this study is the averaged value, i.e., overestimated near the fusion boundary and underestimated near the weld pool center. Despite of the assumptions made for $G_L$, the experimental findings can be adequately explained in the present study. The $G_L$ range was determined to be 0.22–0.37 K $\mu m^{-1}$ and 0.29–0.43 K $\mu m^{-1}$ for the ǁ-U and ǁ-D welds, respectively. Larger dimension of the ǁ-U weld produced the smaller range of the $G_L$. The perpendicular weld had a $G_L$ range of 0.29–0.43 same as the ǁ-D weld, because they had nearly same penetration and width of the weld pool. As a result, small weld pool dimension in the ǁ-D weld produced the larger $G_L$ than that of the ǁ-U weld. This implies that the ǁ-D weld has more columnar structure near the surface and the ǁ-U weld loses the columnar structure.

In summary, it appears that the shape of the s-l interface associated with convection flows significantly influences the $V_S$ and $G_L$ for the welding conditions considered in this study. In the ǁ-D weld, the abnormal 'S' shape of the solidification orientation was associated with the receded s-l interface due to the inhibited convection flow. The morphological behavior of the weld solidification as a function of gravitational orientation is tabulated as follows:

- ǁ-U orientation → larger weld pool → smaller thermal gradient ($G_L$) and more significant convection flow → less columnar microstructure near the weld surface,
- ǁ-D orientation → smaller weld pool → larger thermal gradient ($G_L$) and weaker convection flow → more columnar microstructure near the weld surface.

This confirms the hypothesis postulated in the beginning of Section 3 along with experimental findings.

### 3.3. Primary dendrite spacing

Effects of gravitational orientation on the grain substructure were investigated because the variation of solidification morphology and convection flows plays a role in modifying the microstructural size [33]. Fig. 7 shows the measured primary dendrite spacing ($\lambda_1$) in the longitudinal cross-section through the thickness. Regardless of the welding orientation, the $\lambda_1$ was at its coarsest near the fusion boundary and it became finer approaching the weld pool surface. The ǁ-U weld exhibited approximately 18% larger averaged $\lambda_1$ both near the fusion boundary and weld pool surface, compared with that of the ǁ-D and the ⊥ welds. It was observed that the ǁ-D and the ⊥ welds had almost the same $\lambda_1$ values. This result is probably because of the slower cooling

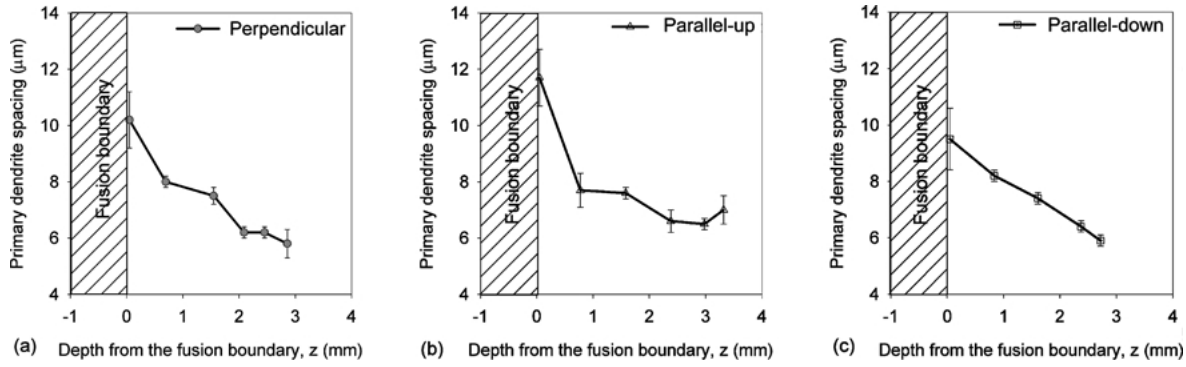


*Figure 7* The primary dendrite spacing ($\lambda_1$) measured as a function of welding orientation: (a) perpendicular, (b) parallel-up, and (c) parallel-down.

rate in the ll-U weld. The ll-U weld had approximately 22% larger weld pool area while the welding power remained constant for all experiments. It suggests that the slower cooling rate in the ll-U weld will have a longer time for the diffusion and coarsening, therefore producing the larger microstructural size. The ll-D weld showed an abnormal 'S' shape of the $V_S$ in the previous Section. However, the $\lambda_1$ decreased continuously from the boundary to the surface similar to the primary spacing in $\perp$ and ll-U welds. To understand normal behavior of the $\lambda_1$ and abnormal behavior of the $V_S$ in the ll-D weld, it is necessary to investigate the independent roles of $G_L$ and $V_S$ on the $\lambda_1$ using Equations 1 and 2.

Although convection is known to have a significant role in influencing the microstructural characteristics [21, 33], its effects were ignored in driving Equations 1 and 2. In unidirectional solidification of Al-Cu alloys, well-developed dendrites were observed in microgravity due to the absence of gravity-driven convection. This resulted in larger primary dendrite spacing ($\lambda_1$) and longer dendrites [6]. However, the smaller $\lambda_1$ in the ll-D weld is not comparable with the previous results [6] because the larger $\lambda_1$ is expected to form as a result of the weak convection. The argument in the $\lambda_1$ between the ll-U and ll-D welds seems to be related to the morphological variation. As the solidification proceeded from the boundary to the surface, the columnar morphology remained near the surface for the ll-D weld. However, its directionality was fading out for the ll-U weld. Therefore, the smaller $\lambda_1$ in the ll-D weld is partly due to the more columnar structure in morphology and partly due to the variation of $G_L$ and $V_S$, which will be discussed next.

Effects of the solidification parameters ($G_L$ and $V_S$) on the $\lambda_1$ behavior were investigated with respect to various welding orientation. The $G_L$ and $V_S$ were determined in the previous section depending on the resultant weld pool shape and the solidification orientation, respectively. A relation between the size of the dendritic substructure and the conditions under which solidification takes place in the unidirectional solidification has been well established. Theoretical models have been proposed to examine the influence of solidification parameters on the microstructural size, specifically $\lambda_1$, by Hunt [18], Kurz and Fisher [19], and Trivedi [20]. Their theoretical models for the $\lambda_1$ are very similar and the only difference among them is a constant $C_1$ in Equation 1. For the high solidification rates, Equation 2 was found to fit reasonably with the measured $\lambda_1$. To use Equations 1 and 2, it is necessary to have the weld solidification in the steady state. In the weld pool, the rapid acceleration of the interface from a zero solidification rate at the s-l boundary to a maximum value at the surface can make the steady state growth theory inappropriate for the interpretation of the experimental results. However, Zimmermann *et al.* [24] have demonstrated that the quasi-steady state condition is satisfied if the incremental change in $V_S$ is much less than $V_S$, when the interface moves through a distance $D\ V_S^{-1}$. $D$ is diffusion coefficient in liquid and it will be indicated later in Table III. This condition was easily satisfied over the entire depth of a welded track as indicated in Equation 4.

$$\frac{\frac{D}{V_S} \cdot \frac{\delta V_S}{\delta x}}{V_S} \ll 1. \tag{4}$$

The $\lambda_1$ behavior on the $V_S$ was investigated for various gravitational orientations. Fig. 8 shows the log scale of $\lambda_1$ behavior including a linear regression result. The linear regression analysis on the $\lambda_1$ behavior is based on the previous work done by Gremaud *et al.* [23]; the $G_L$ effects on the $\lambda_1$ could be safely ignored because the solidification rate ($V_S$) is known to be the key variable in microstructure selection under rapid solidification conditions. Although this assumption conflicts with significant $G_L$ influences on the solidification morphology mentioned in the previous section, it showed a fairly good agreement of the fitted lines with the experimental $\lambda_1$ values for the $\perp$ and ll-U welds. The $\lambda_1$ of the ll-D weld (Fig. 8c) showed a large scatter compared with the regression line, which was associated with the abnormal 'S' shape of the $V_S$. Except for the $\lambda_1$ at $V_S = 2.2$ mm s$^{-1}$, the fitted line also showed a good agreement with the experimental $\lambda_1$. The exponent $b$ ($= 0.54$) for the $\perp$ weld was in a good agreement with the previous experimental relation ($\lambda_1^2\ V_S =$ constant) as shown in Equation 2. The ll-D weld showed clearly smaller exponent $b$ ($= 0.38$) than that for the ll-U weld ($b = 0.61$). The $\lambda_1$ in the ll-U orientation was more significantly affected by the $V_S$ variation than that in the ll-D orientation.

Variation of $G_L$ and $V_S$ for the hypoeutectic Al based-alloys is summarized in Table II including the results of

TABLE II Variation of microstructural parameters ($\lambda_1$) with solidification parameters ($G_L$ and $V_S$) for hypoeutectic Al-Cu alloys

| Composition | $G_L$ (K mm$^{-1}$) | $V_S$ ($\mu$m s$^{-1}$) | $a$ | $b$ | References |
|---|---|---|---|---|---|
| Al-2 wt% Cu | 7.5 | 30–440 | – | 0.5 | [15] |
| Al-3 wt% Cu | 1–5.5 | 8–490 | 0.41 | 0.32 | [14] |
| Al-4.1 wt% Cu | 4 | 0.2–70 | – | 0.4 | [16] |
| Al-4.4 wt% Cu | 0.8–10 | 50–500 | 0.5 | 0.36 | [14] |
| Al-4.5 wt% Cu | 8.8 | 10–240 | – | 0.38 | [13] |
| Al-6 wt% Cu | 1–5.5 | 8–490 | 0.57 | 0.28 | [14] |
| Al-6 wt% Fe | – | 90E3–520E3 | – | 0.54 | [24] |
| Al-4 wt% Cu ($\perp$) | 150–380 | 800–3000 | – | 0.54 | This study |
| Al-4 wt% Cu (II-U) | 150–380 | 800–3000 | – | 0.61 | This study |
| Al-4 wt% Cu (II-D) | 150–380 | 800–3000 | – | 0.38 | This study |

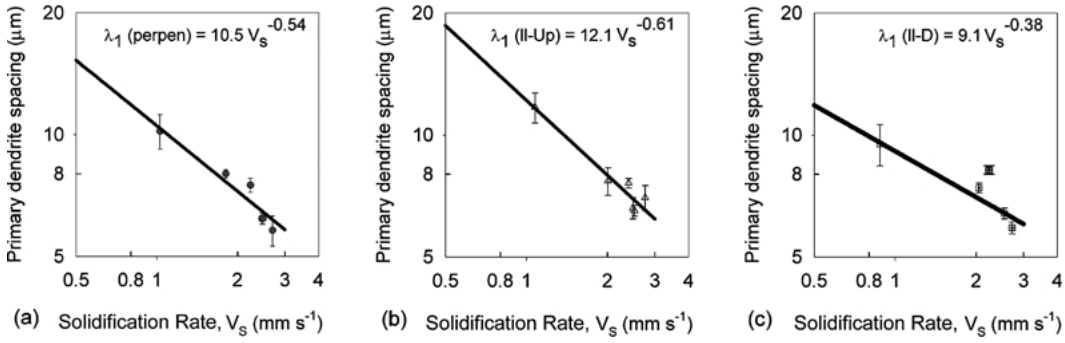


*Figure 8* Effects of gravitational orientation on the $\lambda_1$ behavior for the (a) $\perp$, (b) II-U, and (c) II-D weld as a function of $V_S$.

present studies for the purpose of comparison. A good agreement of the $\lambda_1$ fitted lines with respect to the $V_S$ shows that the $G_L$ variation along the s-l interface may not be significant on the $\lambda_1$ and rapid solidification conditions can be applied to the present study. However, the $G_L$ contribution with respect to gravitational orientation should not be ignored on the $\lambda_1$ behavior based on the significantly different pre-exponential constants, i.e., 10.5 for the $\perp$, 12.1 for the II-U, and 9.1 for the II-D. This $G_L$ effect on the $\lambda_1$ will be discussed later in this section combining with the $V_S$ effect. The theoretical model with no consideration of convection flows indicates the exponent $b = 0.25$ as shown in Equation 1, which is closer to the $b$ value for the II-D weld. Therefore, the II-D weld will have relatively less convection flows compared with the II-U weld. This result also confirms with the morphological behavior, i.e., appearance of more columnar structure near the surface in the II-D weld.

To predict the $\lambda_1$ values quantitatively, combined effects of the $G_L$ and $V_S$ on the $\lambda_1$ analysis were further incorporated in Equation 1. It is worth mentioning that the exponent $a$ ($=0.5$) is larger than the exponent $b$ ($=0.25$) in the theoretical model of Equation 1. The constant $C_1$ in Equation 1 followed Hunt model [18],

$$C_1 = 2.83[m(k_e - 1)D\Gamma C_o]^{0.25} \quad (5)$$

where $m$ is liquidus slope, $k_e$ is equilibrium partition coefficient, $D$ is diffusion coefficient in liquid, $\Gamma$ is Gibbs-Thomson coefficient, and $C_o$ is the alloying composition. The constants used in the calculation are indicated in Table III. Among the models such as Hunt model [18], Kurz-Fisher model [19], and Trivedi model [20], the Hunt model produced a good agreement with the experiments under the welding conditions of the present study. The agreement with the Hunt model is indicated in Fig. 9 and this result is comparable with the previous study on directional solidification of Al-Cu alloys [14]. Furthermore, Choi *et al.* showed that the range of predicted $\lambda_1$ using Equation 1 was in agreement with the experimental values for 304 stainless steel welds [38].

Fig. 9 shows the $\lambda_1$ relation between the experiments and the theoretical models considering a varying $G_L$ both for the welding orientation and along the trailing s-l interface. The model calculation used the $V_S$ measured from the solidification orientation (Fig. 5b) and the $G_L$ estimated from the weld pool shape (Fig. 6) in Equation 1. Regardless of the welding orientation, the experimentally observed values of $\lambda_1$ agreed more reasonably with the Hunt model. Larger $\lambda_1$ for the II-U weld was also predicted than that for the $\perp$ and II-D weld, in which the II-U weld had the smaller $G_L$ range compared with the other welds. However, it is not evident in Fig. 9 due to its large scale in the y-axis. For this investigation of $G_L$ and $V_S$ effects on the $\lambda_1$ behavior,

TABLE III Physical constants of Al-Cu alloys under investigation [14, 24]

| Parameters | Value |
|---|---|
| Overall alloy composition ($C_o$) | 4 wt% |
| Equilibrium partition coefficient ($k_e$) | 0.14 |
| Pre-exponential constant ($D_o$) | $1.1 \times 10^{-7}$ m$^2$ s$^{-1}$ |
| Activation energy for diffusion | 23.8 kJ mol$^{-1}$ |
| Liquidus slope ($m$) | $-2.73$ K wt%$^{-1}$ |
| Gibbs-Thomson coefficient ($\Gamma$) | 0.241 K $\mu$m |

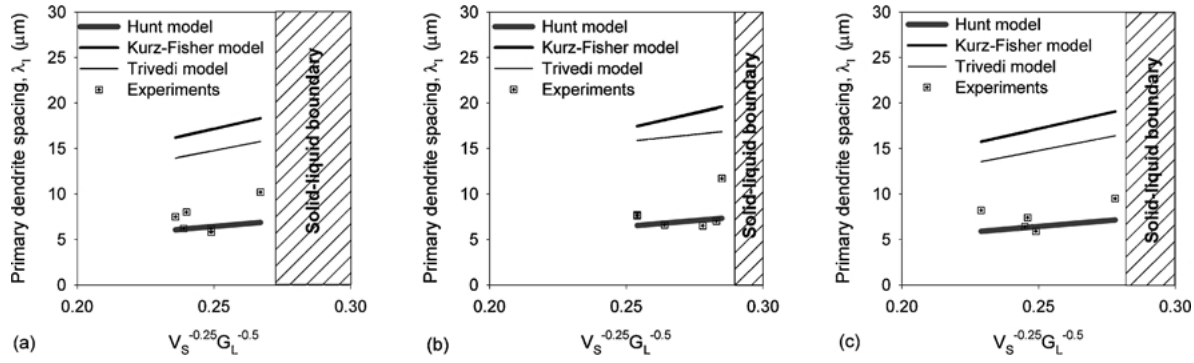


*Figure 9* Comparison of $\lambda_1$ obtained from the experiments and with theoretical models for various welding orientation: (a) ⊥ weld, (b) ll-U, and (c) ll-D weld.

quite large scatters were observed between the model prediction and the experimental findings. That is probably because the convection effects were not included in the theoretical model and the large scatters during the $\lambda_1$ measurement were observed in the longitudinal cross-section, which was discussed in the previous section. Despite the large scatters in Fig. 9, the Hunt model predicted the $\lambda_1$ values associated with the $G_L$ and $V_S$ variation within a fairly reasonable range.

In summary, the $\lambda_1$ analysis with neglecting the $G_L$ variation showed a reasonable agreement with the experimental $\lambda_1$ except for the abnormal $\lambda_1$ behavior in the ll-D weld. Normal welding orientation (perpendicular) showed a good agreement with the relation $\lambda_1^2 V_S =$ constant. However, the $\lambda_1$ in the ll-U was more significantly affected by the $V_S$ based on the larger exponent $b$ compared to that in the ll-D. The abnormal $\lambda_1$ behavior in the ll-D weld might have occurred from the abnormal 'S' shape of the $V_S$ variation. Regardless of the welding orientation, the Hunt model could reproduce quantitatively the $\lambda_1$ values within a fairly reasonable range. The larger $\lambda_1$ in the ll-U weld pool surface might be associated with a morphological change and a variation of both $V_S$ and $G_L$. This result also confirms the authors' findings and the hypothesis postulated in the beginning of the Section 3.

## 4. Conclusions

The GTA weld microstructure on Al-4 wt% Cu alloy was investigated to determine the impact of gravitational orientation on the weld solidification behavior. This was accomplished through GTA welding and an analytical study of the weld microstructure. Using a heat input of relatively high power (185 amperes × 16.5 voltages) and slow arc translation velocity (3 mm $s^{-1}$), bead-on-plate welding experiment was performed under a wide range of observed $V_S$ (0.8–3 mm $s^{-1}$) with a calculated $G_L$ (150–380 K $mm^{-1}$). The ll-U weld showed 22 percent larger weld pool area than that of the ⊥ and ll-D welds. Larger $\lambda_1$ in the ll-U weld was observed near the weld pool surface and the fusion boundary than the case of ⊥ and ll-D welds. This was because of the morphological change (loss of the columnar structure) and the smaller $G_L$ range induced by larger weld pool dimensions. The ll-D weld exhibited different solidification morphology, e.g., more columnar structure near the weld pool surface and abnormal 'S' shape of the solidification rate during its growth. This result might be associated with relatively mild convection flows and receded s-l interface due to the gravity, respectively. Hunt model predicted the trend of $\lambda_1$ as a function of gravitational orientation. However, it is concluded that, based on quantitative comparison, a better model is needed that can reflect the effects of gravitational orientation. In summary, the gravitational orientation changed the weld pool shape associated with convection flows. This variation on the convection flow influenced the shape of the trailing s-l interface. Therefore, the solidification morphology and primary dendrite spacing ($\lambda_1$) were modified because the solidification rate ($V_S$) and thermal gradient ($G_L$) were affected by the convection flow.


## Acknowledgements

The authors acknowledge the financial support by NASA Materials Microgravity Division under the Grant NAG8-1272.


## References


1. K. NOGI, Y. AOKI, H. FUJII and K. NAKATA, *Acta Materialia* **46**(12) (1998) 4405.
2. J. S. FOLEY and C. M. BANAS, *ICALEO'87* (1987) 47.
3. B. E. PATON, *Autom. Weld.* **25**(6) (1972) 1.
4. D. K. AIDUN, J. J. DOMEY and G. AHMADI, *Welding Journal* **79**(6) (2000) 145s.
5. C. C. BATTAILE, R. N. GRUGEL, A. B. HMELO and T. G. WANG, *Metall. and Mater. Trans.* A **25A** April (1994) 865.
6. H. YU, K. N. TANDON and J. R. CAHOON, *Metall. Trans.* **28A** (1997) 1245.
7. R. P. LIU, J. H. ZHAO, X. Y. ZHANG, D. W. HE, L. L. SUN, Z. C. QIN, Y. F. XU and W. K. WANG, *J. Mater. Sci.* **33** (1998) 2679.
8. K. N. TANDON, F. SAADAT, M. C. CHATURVEDI and J. R. CAHOON, *Microgr. Sci. and Techn.* **VI**(1) (1991) 19.
9. G. L. WORKMAN and W. F. KAUKLER, *ICALEO'90* (1990) 430.
10. D. K. AIDUN and J. P. DEAN, *Welding Journal* **78**(10) (1999) 349s.
11. M. C. FLEMINGS, "Solidification Processing" (McGraw-Hill, New York, 1974).
12. W. KURZ and D. J. FISHER, "Fundamentals of Solidification" (Aedermannsdorf, Switzerland, Trans Tech Publications, 1992).
13. X. LIN, W. HUANG, J. FENG, T. LI and Y. ZHOU, *Acta Mater.* **47**(11) (1999) 3271.

14. M. GÜNDÜZ and E. CADIRLI, *Mater. Sci. and Eng* A**327** (2002) 167.
15. R. M. SHARP and A. HELLAWELL, *J. Cryst Growth* **11** (1971) 71.
16. Y. MIYATA, T. SUZUKI and J. I. UNO, *Metall. Trans.* **16A** (1985) 1799.
17. J. T. MASON, J. D. VERHOEVEN and R. TRIVEDI, *J. Cryst. Growth* **59**(3) (1982) 516.
18. J. D. HUNT, "Solidification and Casting of Metals" (The Metal Society, London, 1979) p. 3.
19. W. KURZ and D. J. FISHER, *Acta Metall.* **29** (1981) 11.
20. R. TRIVEDI, *Metall. Trans.* **15A** (1984) 977.
21. M. RAPPAZ, S. A. DAVID, J. M. VITEK and L. A. BOATNER, *ibid.* **20A**(6) (1989) 1125.
22. W. KURZ, B. GIOVANOLA and R. TRIVEDI, *Acta Metall.* **34** (1986) 823.
23. M. GREMAUD, M. CARRARD and W. KURZ, *Acta Metall et Mater.* **38**(12) (1990) 2587.
24. M. ZIMMERMANN, M. CARRARD and W. KURZ, *Acta Metall.* **37**(12) (1989) 3305.
25. J. A. BROOKS, M. LI and N. C. Y. YANG, *Inst. Mater.* (1997) 184.
26. S. LU, J. D. HUNT, P. GILGIEN and W. KURZ, *Acta Metall. et Mater.* **42**(5) (1994) 1653.
27. N. KANG, T. A. MAHANK, A. K. KULKARNI and J. SINGH, *Mater. and Manuf. Proc.* **18**(2) (2003) 169.
28. R. E. MUELLER, PhD thesis, York University, North York, Ontario, 1994.
29. F. MIYASAKA, T. YOKOGAWA, H. NISHIKAWA, T. OJI, Y. HIRATA and T. MASUTANI, *Weld. Inter.* **13**(7) (1999) 536.
30. J. DOMEY, D. K. AIDUN, G. AHMADI, L. L. REGEL and W. R. WILCOX, *Weld. Journal* **74**(8) (1995) 263s.
31. T. GANAHA, B. P. PEARCE and H. W. KERR, *Metall. Trans.* A **11A**(8) (1980) 1351.
32. S. KOU and D. K. SUN, *ibid.* **16A**(2) (1985) 203.
33. L. S. CHAO and J. A. DANTZIG, in Proceedings of 10th National Congress on Applied Mechanics, Austin, TX, 1986, p. 249.
34. M. GAUMANN and W. KURZ, "Mathematical Modelling of Weld Phenomena 4" (Institute of Materials, 1997) p. 125.
35. O. GRONG, "Metallurgical Modelling of Welding," 2nd ed. (The Institute of Materials, London, 1997) p. 251.
36. J. R. CLARKE, D. C. WECKMAN and H. W. KERR, International Conference on Trends in Welding Research, Pine Mountain, GA, 1998, p. 72.
37. T. ZACHARIA, A. H. ERASLAN, D. K. AIDUN and S. A. DAVID, *Metall. Trans*. B **20B**(10) (1989) 645.
38. J. CHOI and J. MAZUMDER, *J. Mater. Sci.* **37**(10) (2002) 2143.

*Received 4 November 2002*
*and accepted 20 May 2003*